Nonlinear magneto-optical resonances at D_1 excitation of ^{85}Rb and ^{87}Rb in an extremely thin cell

M. Auzinsh,[1,*] R. Ferber,[1] F. Gahbauer,[1] A. Jarmola,[1] L. Kalvans,[1] A. Papoyan,[2] and D. Sarkisyan[2]

[1]*Laser Centre, The University of Latvia, 19 Rainis Boulevard, LV-1586 Riga, Latvia*
[2]*Institute for Physical Research, NAS of Armenia, Ashtarak-0203, Armenia*

Nonlinear magneto-optical resonances have been measured in an extremely thin cell (ETC) for the D_1 transition of rubidium in an atomic vapor of natural isotopic composition. All hyperfine transitions of both isotopes have been studied for a wide range of laser power densities, laser detunings, and ETC wall separations. Dark resonances in the laser induced fluorescence (LIF) were observed as expected when the ground-state total angular momentum F_g was greater than or equal to the excited-state total angular momentum F_e. Unlike the case of ordinary cells, the width and contrast of dark resonances formed in the ETC dramatically depended on the detuning of the laser from the exact atomic transition. A theoretical model based on the optical Bloch equations was applied to calculate the shapes of the resonance curves. The model, which had been developed previously for ordinary vapor cells, averaged over the contributions from different atomic velocity groups, considered all neighboring hyperfine transitions, took into account the splitting and mixing of magnetic sublevels in an external magnetic field, and included a detailed treatment of the coherence properties of the laser radiation. Such a theoretical approach had successfully described nonlinear magneto-optical resonances in ordinary vapor cells. However, to describe the resonances in the ETC, key parameters such as the ground-state relaxation rate, excited-state relaxation rate, Doppler width, and Rabi frequency had to be modified significantly in accordance with the ETC's unique features. The level of agreement between the measured and calculated resonance curves achieved for the ETC was similar to what could be accomplished for ordinary cells. However, in the case of the ETC, it was necessary to fine-tune parameters such as the background and the Rabi frequency for different transitions, whereas for the ordinary cells, these parameters were identical for all transitions.

PACS number(s): 32.60.+i, 32.80.Xx, 32.10.Fn

I. INTRODUCTION

Atomic vapors confined between walls separated by only a few hundred nanometers have the potential for interesting applications in magnetometry and optoelectronics [1,2]. Spectroscopic cells that have two walls separated by a distance that is on the order of the wavelength of visible or near infrared light are known as extremely thin cells (ETCs) [3]. If the laser radiation propagates in a direction perpendicular to the ETC walls, fluorescence will be observed preferentially from those atoms whose velocity vectors have a small normal component with respect to the walls, since atoms flying rapidly toward an ETC wall will collide with it before being able to fluoresce. As a result, sub-Doppler spectroscopic resolution can be achieved in an ETC [3]. This useful feature can be exploited to study physical phenomena in atomic systems with hyperfine manifolds that are not resolved under normal conditions, such as resonances at zero magnetic field in a plot of laser-induced fluorescence (LIF) versus magnetic field. These resonances can be dark [4,5] or bright [6]. They arise when at zero magnetic field the ground-state magnetic sublevels form a quantum superposition state, which is not coupled to the exciting laser field in the case of dark resonances but coupled strongly in the case of bright resonances. Although the theoretical description of these resonances is straightforward in principle, the theoretical calculations have failed at times to reproduce accurately the experimental signals, in part, because in most available systems the excited-state hyperfine levels were not resolved under Doppler broadening. The

development of the ETC offered a way to address this issue, because the ETC makes possible sub-Doppler resolution. This approach was taken by Andreeva and coworkers [7] for the case of cesium. However, the results contained some surprises in that some resonances that would be bright in an ordinary cell appeared dark in the ETC.

The goal of the present study was to obtain experimental resonance signals with an ETC for the rubidium D_1 transition with high accuracy and as a function of several well-defined parameters. Then, we planned to apply to these data a theoretical model that had been developed to describe nonlinear magneto-optical resonances in ordinary vapor cells [8,9] to see if we could obtain an adequate theoretical description of bright and dark resonances in ETCs with this model.

Nonlinear magneto-optical resonances (see, for example, the review article by Budker *et al.* [10]) are closely related to the ground-state Hanle effect, which was first observed by Lehmann and Cohen-Tannoudji in 1964 [11]. Schmieder [5] and later Alzetta [4] observed dark resonances in alkali metal atoms. The first observations of coherence resonances by means of lasers rather than spectral lamps were carried out by Ducloy *et al.* [12] in fluorescence and by Gawlik *et al.* [13] in connection with the nonlinear Faraday effect. In 1978, Piqué successfully applied a theoretical model based on the optical Bloch equations to describe measurements of dark resonances in the $F_g = 2 \rightarrow F_e = 1$ transition of the D_1 line in a beam of sodium atoms [14]. In 2000, Dancheva *et al.* [6] observed bright resonances for the first time in the D_1 and D_2 transitions of rubidium in an atomic vapor. A theoretical model [15] based on the optical Bloch equations was applied to the experimental study of bright and dark resonances in the D_2 transition of

cesium observed in a vapor cell. [16]. However, the calculations predicted a bright resonance for the $F_g = 4 \rightarrow F_e = 3, 4, 5$ transition, whereas for linearly polarized excitation it appeared to be dark in the experiment. Andreeva *et al.* [7] studied bright and dark resonances in ETCs and suggested that spin-changing collisions of the atoms with the walls could change some bright resonances into dark resonances.

Our initial approach [8,9] to the difficulties in describing bright and dark resonances in atomic vapors was to develop further a theoretical model [15] that would take into account the Doppler effect. Besides averaging over the Doppler profile, the model also accounted for all nearby hyperfine transitions, the splitting and mixing of the magnetic sublevels in the magnetic field, and the coherence properties of the laser radiation. We applied such a model first to the cesium D_1 transition [8], which is almost resolved under Doppler broadening, and then to the rubidium D_1 transition [9], which is partially resolved. The model was successful in describing experimentally measured resonances in ordinary cells for a wide variety of laser power densities, beam diameters, and laser frequency detunings. It required only a few parameters to be adjusted. These parameters were the conversion between the Rabi frequency and the laser power density, the conversion between the laser beam diameter and the ground-state relaxation time, and the percentage of background from scattered LIF. Once the parameters were determined, the same values were used for all data sets. This model served as the starting point of our efforts in the present study to describe bright and dark resonances in the ETC.

The level scheme of the D_1 line in ^{85}Rb and ^{87}Rb is shown in Fig. 1. The allowed transitions between the ground and excited states are represented by the arrows with the relative transition strengths given by the fractions next to the arrows. The energy difference between the excited-state hyperfine levels is 361.6 MHz for ^{85}Rb [17] and 814.5 MHz for ^{87}Rb [18]. In an ordinary vapor cell, the full width at half maximum (FWHM) of the Doppler broadening for the rubidium D_1 transition at room temperature would be about 500 MHz. In the ETC, however, the Doppler broadening is reduced, because atoms flying parallel to the walls are more likely to be observed in the experiment. The LIF excitation spectra of the D_1 line of natural rubidium for both an ordinary vapor cell and an ETC are shown in Fig. 2. In the ordinary cell, the two excited-state hyperfine levels of ^{87}Rb are almost resolved under Doppler broadening,
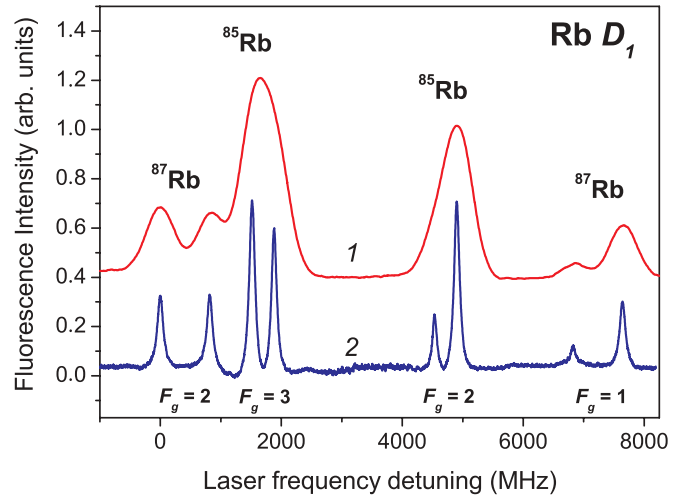
FIG. 2. (Color online) LIF excitation spectra of the Rb D_1 line. Curve 1: in an ordinary cell at 10 mW/cm^2 excitation; curve 2: in an ETC at 10 mW/cm^2 excitation and wall separation $L = \lambda/2$, where λ is the wavelength of the laser radiation.

but the hyperfine levels of ^{85}Rb are practically unresolved. In the ETC, however, each transition can be distinguished easily.

II. EXPERIMENT

The ETC was produced at the Institute of Physical Research in Ashtarak, Armenia, while the experiments described here were performed in Riga. The principle of the ETC is described in Refs. [1,3]. Basically, it consists of two perfectly polished window wafers made from YAG crystal that are glued in such a way that their internal separation varies from 50 nm to about 1.8 μm. Rubidium is stored in a sapphire tube bonded to the YAG windows and terminated by a small glass tube extension which makes it possible to fill the cell with rubidium and seal it. The cell was operated in a two-chambered oven, which keeps the YAG windows at about 200°C and the rubidium arm at about 150°C. The laser was a DL 100 external-cavity single mode diode laser with a wavelength of 794.3 nm and a typical linewidth of a few megahertz, which was produced by Toptica, A. G., of Graefelfing, Germany. The laser beam passed through a Glan-Thompson polarizer before entering the cell. The cell was placed at the center of a three-axis Helmholtz coil system, which rested on a nonmagnetic optical table. Two pairs of coils compensated the laboratory magnetic field, while the third pair of coils was used to scan the magnetic field in the observation direction. The current in this third pair of coils was scanned with a Kepco BOP-50-8M bipolar power supply, which was controlled by an analog signal from a computer. Figure 3 depicts the relative orientation of the laser beam (exc), the laser radiation's linear polarization vector ($\mathbf{E}_{exc}$), the magnetic field ($\mathbf{B}$), the observation direction (obs), and the ETC walls. The experimental setup and auxiliary equipment were similar to what was used in Ref. [8]. Data was acquired with a National Instruments 6024E data acquisition card.

The LIF was detected by means of a Thorlabs FDS-100 photodiode as a function of magnetic field for all hyperfine transitions of the two isotopes of rubidium (see Fig. 1). Fluorescence emerged through the side walls of the ETC.
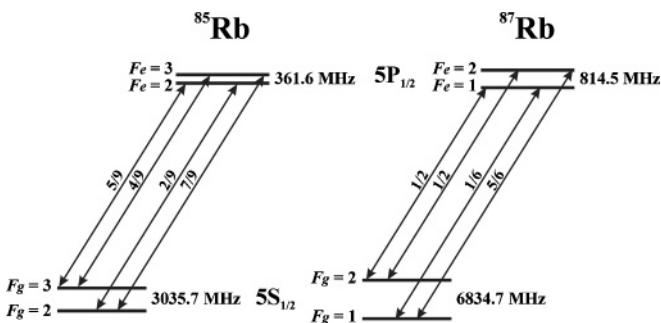

FIG. 1. Hyperfine level structure and transitions of the D_1 line of rubidium. The fractions on the arrows indicate the relative transition strengths [17,18].
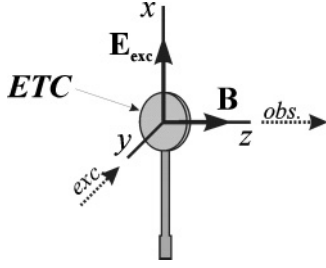
FIG. 3. Experimental geometry. The relative orientation of the laser beam (exc), laser light polarization ($\mathbf{E}_{\text{exc}}$), magnetic field ($\mathbf{B}$), observation direction (obs), and ETC walls are shown.

No polarizers were used in the LIF observation. Signals were obtained for various laser power densities between 10 and 2000 mW/cm^2. The laser beam diameter was usually 0.44 mm (FWHM of intensity), as measured by a Thorlabs BP 104-VIS beam profiler, but different laser beam diameters were also applied to the cell.

To record the signal, the laser's frequency was maintained at the value that gave the maximum fluorescence signal for a given transition at zero magnetic field. The fluorescence was recorded while the magnetic field was scanned several times, and the scans were averaged. The laser was not actively stabilized, but its frequency was monitored with a High Finesse WS-7 wavemeter. In order to study the dependence of resonance shapes on laser detuning, for some observations we used a double scanning technique [19], in which the laser frequency was scanned slowly across a transition while the magnetic field was scanned more rapidly from negative to positive values with a triangular waveform. The laser frequency changed by about 2–5 MHz/s. The typical laser frequency scan lasted about 1–2 min, whereas the typical period for the magnetic field scan was 1 s. In this manner, a series of resonance signals at laser frequencies differing by 2–5 MHz could be obtained.

In addition to the signal, each measurement included a certain amount of background. Background from scattered laser light was determined for each measurement by tuning the laser off resonance. However, there was an additional background associated with scattered LIF, which could not be readily identified. Studies in the ordinary cell had suggested that this background accounts for a fixed percentage of the signal for a given vapor cell. However, it is also possible that the background differs according to which isotope is studied, since the total amount of fluorescence changes. Furthermore, the background from scattered LIF will likely depend on the thickness of the cell. Its value can be high because fluorescence observed by the detector can be reflected by the walls of the ETC or scattered while passing through the glue that held the walls together (see Fig. 3). The value of this background was one of the parameters that had to be adjusted to find the best fit between experiment and theory.

III. THEORY

A theoretical model had been developed previously in order to describe bright and dark resonances in ordinary vapor cells [8,9], and a detailed description of this theoretical model can be found in these references. We summarize it here

briefly. The model describes the internal atomic dynamics by a semiclassical atomic density matrix ρ, which depends parametrically on the classical coordinates of the atomic center of mass. The time evolution of the density matrix ρ follows the optical Bloch equations (OBEs) [20]:

$$i\hbar\frac{\partial\rho}{\partial t} = [\hat{H}, \rho] + i\hbar\hat{R}\rho. \tag{1}$$

The relaxation operator $\hat{R}$ includes the spontaneous emission rate, which equals the natural transition linewidth Γ_N, and the ground-state relaxation rate γ_g, which in the case of the ETC corresponds to the rate of collisions with the cell wall. We also introduced an excited-state relaxation rate γ_e related mostly to wall interactions in the ETC, which was negligible in the ordinary cell. The Hamiltonian $\hat{H}$ is given by $\hat{H} = \hat{H}_0 + \hat{H}_B + \hat{V}$. $\hat{H}_0$ is the unperturbed atomic Hamiltonian and depends on the internal atomic coordinates, $\hat{H}_B$ is the Hamiltonian of the atomic interaction with the magnetic field, and $\hat{V} = -\hat{\mathbf{d}} \cdot \mathbf{E}(t)$ is the dipole interaction operator.

Taking into account the classical motion of the atoms, the resulting Doppler shifts, and the coherent properties of the laser radiation, we apply the rotating wave approximation [21] to the OBEs. This approximation yields stochastic differential equations, which can be further simplified by using the decorrelation approach [22]. Since the experimentally observed light intensity is averaged over time intervals that are large compared to the characteristic time of the phase fluctuations, it is permissible to average over the stochastic differential equations following the method described in Ref. [15] and references therein.

After adiabatically eliminating the density matrix elements that correspond to optical coherences, we arrive at the equations for the Zeeman coherences:

$$
\begin{aligned}
\frac{\partial\rho_{g_ig_j}}{\partial t} &= \left(\Gamma_{p,g_ie_m} + \Gamma^*_{p,e_kg_j}\right)\sum_{e_k,e_m}\left(d_1^{g_ie_k}\right)^*d_1^{e_mg_j}\rho_{e_ke_m} \\
&\quad - \sum_{e_k,g_m}\left[\Gamma^*_{p,e_kg_j}\left(d_1^{g_ie_k}\right)^*d_1^{e_kg_m}\rho_{g_mg_j}\right. \\
&\quad \left. + \Gamma_{p,g_ie_k}\left(d_1^{g_me_k}\right)^*d_1^{e_kg_j}\rho_{g_ig_m}\right] - i\omega_{g_ig_j}\rho_{g_ig_j} \\
&\quad + \sum_{e_i,e_j}\Gamma^{e_ie_j}_{g_ig_j}\rho_{e_ie_j} - \gamma_g\rho_{g_ig_j} + \lambda\delta(g_i, g_j)
\end{aligned} \tag{2}
$$

and

$$
\begin{aligned}
\frac{\partial\rho_{e_ie_j}}{\partial t} &= \left(\Gamma^*_{p,e_ig_m} + \Gamma_{p,g_ke_j}\right)\sum_{g_k,g_m}d_1^{e_ig_k}\left(d_1^{g_me_j}\right)^*\rho_{g_kg_m} \\
&\quad - \sum_{g_k,e_m}\left[\Gamma_{p,g_ke_j}d_1^{e_ig_k}\left(d_1^{g_ke_m}\right)^*\rho_{e_me_j} + \Gamma^*_{p,e_ig_k}d_1^{e_mg_k}\right. \\
&\quad \left. \times \left(d_1^{g_ke_j}\right)^*\rho_{e_ie_m}\right] - i\omega_{e_ie_j}\rho_{e_ie_j} - \Gamma\rho_{e_ie_j}.
\end{aligned} \tag{3}
$$

In these equations $\rho_{g_ig_j}$ and $\rho_{e_ie_j}$ are the density matrix elements for the ground and excited states, respectively. The first term in (2) describes the repopulation of the ground state and the creation of Zeeman coherences from induced transitions; Γ_{p,g_ie_j} and Γ^*_{p,e_ig_j} are the couplings between the laser field and the ground and excited states; and $d_1^{e_ig_j}$ is the dipole transition matrix element between the ground state i and the excited state j. The second term contains the changes of

the ground-state Zeeman sublevel population and the creation of ground-state Zeeman coherences after light absorption. The third term describes the destruction of the ground-state Zeeman coherences by the external magnetic field; $\omega_{g_i g_j}$ is the splitting of the ground-state Zeeman sublevels. The fourth term describes the repopulation and transfer of excited-state coherences to the ground state as a result of spontaneous transitions. We assume our transition to be closed (within the fine structure, all atoms undergoing spontaneous transitions return to the initial fine structure state $5S_{1/2}$), and so $\sum_{e_i,e_j} \Gamma_{g_i g_j}^{e_i e_j} = \Gamma_N$, the natural linewidth. The fifth and sixth terms show the relaxation and repopulation of the ground state due to nonoptical reasons; in our case it is assumed to be solely ground-state relaxation due to wall collisions. We assumed that the atomic equilibrium density outside the interaction region is normalized to 1 and so $\lambda = \gamma_g$.

In Eq. (3) the first term describes the light absorbing transitions; the second term denotes induced transitions to the ground state; the third describes the destruction of ground-state Zeeman coherences in the external magnetic field, where $\omega_{e_i e_j}$ is the splitting of the excited-state Zeeman sublevels; and the fourth term denotes the rate of spontaneous decay of the excited state. The excited-state decay rate is given by $\Gamma = \Gamma_N + \gamma_e$, where Γ_N is the natural linewidth and γ_e represents the relaxation rate of the excited state, which results mostly from interactions with the ETC walls.

The interaction strength $\Gamma_{p,g_i e_j}$ is given by

$$\Gamma_{p,g_i e_j} = \frac{\Omega_R^2}{\left[\left(\frac{\Gamma_N}{2} + \frac{\Delta\omega}{2} \right) \pm i \left(\overline{\omega} - \boldsymbol{k}_{\overline{\omega}} \boldsymbol{v} - \omega_{e_j g_i} \right) \right]}, \quad (4)$$

where $\overline{\omega}$ is the central laser frequency, $\Delta\omega$ is the laser linewidth, and the squared Rabi frequency Ω_R^2 is proportional to the laser power density.

The magnetic field not only splits the Zeeman sublevels by an amount ω_{ij} but also changes the transition dipole elements by mixing the magnetic sublevels. The Breit-Rabi formula [23,24] gives the mixing in the case of two hyperfine levels. Although the ground-state hyperfine levels are separated by several gigahertz, all four hyperfine components were taken into account simultaneously to model the experimental signals. As can be seen from Eq. (4), absorption is possible from both hyperfine levels in one experiment when taking into account the natural linewidth of the optical transition, the Doppler line shift, and the laser detuning from the exact resonance.

The experiments are assumed to take place under stationary excitation conditions so that $\partial \rho_{g_i g_j}/\partial t = \partial \rho_{e_i e_j}/\partial t = 0$. Thus, one can reduce the differential equations (2) + (3) to a system of linear equations and solve it to obtain the density matrices for the atomic ground and excited states. From the density matrices, one obtains the observed fluorescence intensity as follows:

$$I_f(\tilde{\mathbf{e}}) = \tilde{I}_0 \sum_{g_i,e_i,e_j} d_{g_i e_j}^{(ob)*} d_{g_i e_i}^{(ob)} \rho_{e_i e_j}, \quad (5)$$

where $\tilde{I}_0$ is a constant of proportionality.

The signal is integrated over the different atomic velocity groups and summed over the two orthogonal polarization components of the fluorescence and over all nearby hyperfine transitions, including both ground-state hyperfine levels.

The above model initially was developed for vapor cells of ordinary dimensions. However, the geometry of the ETC differs substantially from an ordinary cell. In particular, the atoms are confined between very narrow walls, which could affect the dynamics of the excitation and relaxation processes. For example, in the ordinary cell, the ground-state relaxation rate γ_g is related to the beam diameter and is usually on the order of a few tens of kilohertz. In the ETC, however, atoms will collide with the wall of the ETC much more frequently. Taking into account the Doppler width estimated from Fig. 2 and the wall separation, one can expect ground-state relaxation rates on the order of several megahertz in the ETC.

Figure 4 shows the results for two transitions of ^{87}Rb of theoretical calculations that were performed to study the impact on the resonance shapes of various parameters that might depend on wall thickness in the ETC. Except as otherwise indicated in the figures, the Rabi frequency used in the calculations was $\Omega_R = 6.45$ MHz, and the ground-state relaxation rate was $\gamma_g = 3$ MHz. The excited-state relaxation rate was $\gamma_e = 20$ MHz, except in Fig. 4(a), where it was close to zero for $\gamma_g = 0.03$ MHz and increased to $\gamma_e = 20$ MHz for $\gamma_g = 3.0$ MHz. The Doppler width was assumed to be 500 MHz for $\gamma_g < 0.3$ and after that decreased linearly to 60 MHz at $\gamma_g = 3.0$ MHz. Larger ground- and excited-state relaxation rates were assumed to be related to smaller wall separation, which favors excitation and fluorescence of atoms that have a small velocity component perpendicular to the walls. As the distance between the ETC walls decreases, the more likely it becomes for atoms to collide with the walls during the atom-light interaction, and so the relaxation rates increase.

Figures 4(a) and 4(b) show effects of changing the ground- and excited-state relaxation rates in the model for the case of a bright and a dark resonance, respectively. A ground-state relaxation rate $\gamma_g = 0.03$ MHz is typical of an ordinary cell, in which γ_e is negligible. In an ETC γ_g on the order of several megahertz and γ_e on the order of 20 MHz could be realistic values when taking into account frequent wall collisions. At slow ground-state relaxation rates, one observes narrow resonances in both cases, although in the case of the bright resonance the contrast is small. As the ground-state relaxation rate increases, the narrow bright resonance at first gets broader and eventually disappears completely, while simultaneously the large-field fluorescence decreases. For the dark resonance, the resonance width increases with increasing ground-state relaxation rate, while the resonance contrast decreases. The large-field fluorescence likewise decreases with increasing ground-state relaxation rate. Figure 4(c) shows the dark resonance for various values of the Rabi frequency Ω_R for $\gamma_g = 3.0$ MHz. Figure 4(c) shows that the resonance contrast, resonance width, and the value at which the fluorescence reaches a maximum all increase with increasing Rabi frequency. Finally, Fig. 4(d) shows the effect on the resonance shapes of varying the excited-state relaxation rate γ_e. The excited-state decay rate may also increase as the wall separation decreases. It can be seen that as the excited-state decay rate increases, the resonance contrast decreases, and fluorescence decreases less steeply at large magnetic field values.

The evolution of these calculated signals qualitatively agrees with the evolution of experimentally measured signals
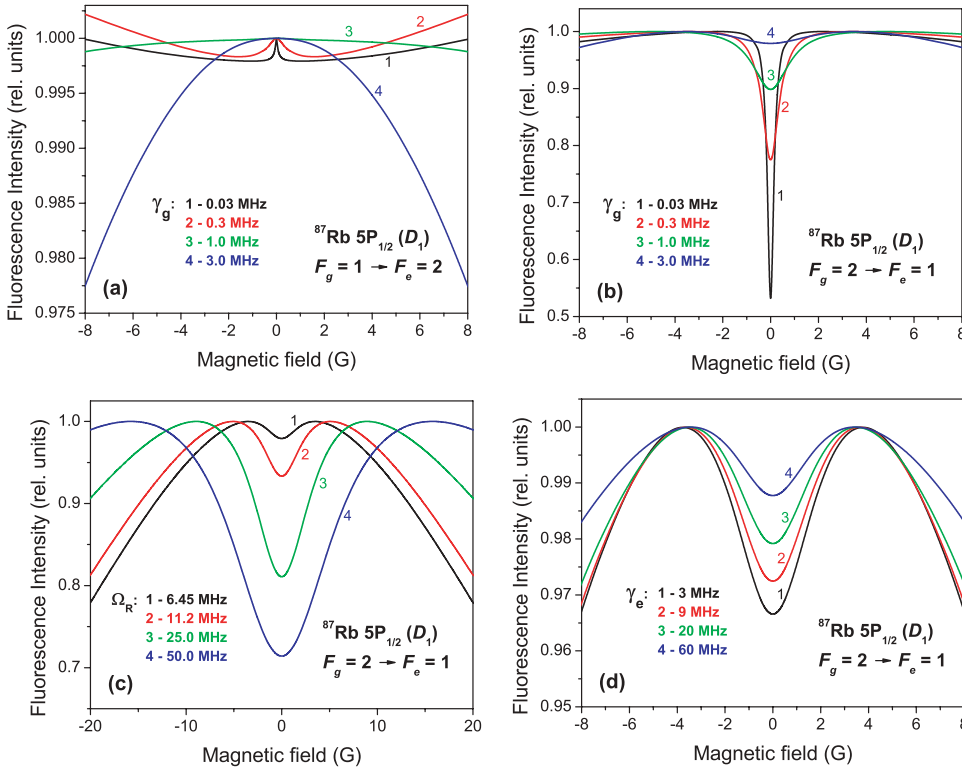
FIG. 4. (Color online) Theoretical predictions of resonance shapes for various values of parameters found in the theoretical model. (a) Bright resonance at the $F_g = 1 \rightarrow F_e = 2$ transition of ^{87}Rb for various values of the ground-state relaxation rate γ_g. (b) Dark resonance at the $F_g = 2 \rightarrow F_g = 1$ transition of ^{87}Rb for different values of the ground-state relaxation rate γ_g. (c) Dark resonance at the $F_g = 2 \rightarrow F_g = 1$ transition of ^{87}Rb for different values of the Rabi frequency Ω_R. (d) Dark resonance at the $F_g = 2 \rightarrow F_g = 1$ transition of ^{87}Rb for different values of the excited-state relaxation rate γ_e.

as one goes from ordinary cells with large laser beam diameters to smaller laser beam diameters (see Ref. [9], Fig. 9) and finally to an ETC, as will become apparent in the next section. We therefore put forth the hypothesis that the resonance shapes in the ETC can be modelled by the same theoretical model that is used in vapor cells of ordinary dimensions, but that it is necessary to adjust the values of the ground-state relaxation rate, excited-state relaxation rate, Doppler width, and Rabi frequency in accordance with the small distance between the ETC cell walls. In order to test this hypothesis, we tried to find consistent relationships among the cell wall separation and laser power density, on the one hand, and the ground-state relaxation rate, excited-state relaxation rate, and Rabi frequency, on the other hand, for a large set of measurements performed on all transitions of the D_1 line for various laser power densities and wall separations. Among the adjustable parameters of the model are the conversion between laser power density I and Rabi frequency Ω_R, the conversion factors between the ETC wall separation and the ground-state relaxation rate γ_g and excited-state relaxation rate γ_e, and the Doppler width, which was different in the ETC from the case of the ordinary cell. The atomic constants used in the model are taken from the compilations by Steck [17,18].

IV. RESULTS AND DISCUSSION

In general, one expects to observe dark resonances if the total ground-state angular momentum F_g is greater than or equal to the total excited-state angular momentum F_e and a bright resonance if $F_g < F_e$ [25–27]. Figures 5 and 6 show magneto-optical resonances for the various hyperfine transitions at the D_1 line of ^{87}Rb and ^{85}Rb, respectively. Markers represent experimental data while the lines are the result of a theoretical calculation. The following parameter

values were assumed in the theoretical model to describe all transitions at cell wall separation $L = \lambda$: the ground-state relaxation rate γ_g was 2.88 MHz, the Doppler width was 60 MHz (FWHM), and the excited-state relaxation rate γ_e was 20 MHz. Furthermore, for all the transitions of ^{87}Rb the relationship between Rabi frequency Ω_R in megahertz and laser power density I in mW/cm^2 was assumed to be $I = 0.25$ mW cm^{-2} MHz$^{-2}\Omega_R^2$ and a background, discussed in Sec. II, from laser induced fluorescence of 50% was assumed. For ^{85}Rb, the relationship $I = 0.8$ mW cm^{-2} MHz$^{-2}\Omega_R^2$ was assumed for the transitions with equal total angular momentum F in the ground and excited states and $I = 0.4$ mW cm^{-2} MHz$^{-2}\Omega_R^2$ for the transitions in which F changed. The background from laser-induced fluorescence was assumed to be 37% for all transitions of ^{85}Rb.

Dark resonances were clearly seen as expected at the $F_g = 2 \rightarrow F_e = 1$, $F_g = 2 \rightarrow F_e = 2$, and $F_g = 1 \rightarrow F_e = 1$ transitions shown in Fig. 5 and at the $F_g = 3 \rightarrow F_e = 2$, $F_g = 3 \rightarrow F_e = 3$, and $F_g = 2 \rightarrow F_e = 2$ transitions shown in Fig. 6, since $F_g \geqslant F_e$. However, neither the $F_g = 1 \rightarrow F_e = 2$ transition in ^{87}Rb nor the $F_g = 2 \rightarrow F_e = 3$ transition in ^{85}Rb gave any indication of either a bright or dark resonance associated with ground-state coherences, even though one might have expected a bright resonance here since $F_g < F_e$. This result is entirely consistent with the predictions of the theoretical model shown in Fig. 4(a). The decrease of the observed fluorescence with increasing magnetic field was related to a loss of excited-state coherence as well as to the fact that at high magnetic fields the energy separation of individual transitions between the Zeeman sublevels exceeded the laser linewidth, and, hence, resonant absorption was reduced.

It has been shown previously in an ordinary rubidium vapor cell that the shape of a nonlinear magneto-optical resonance
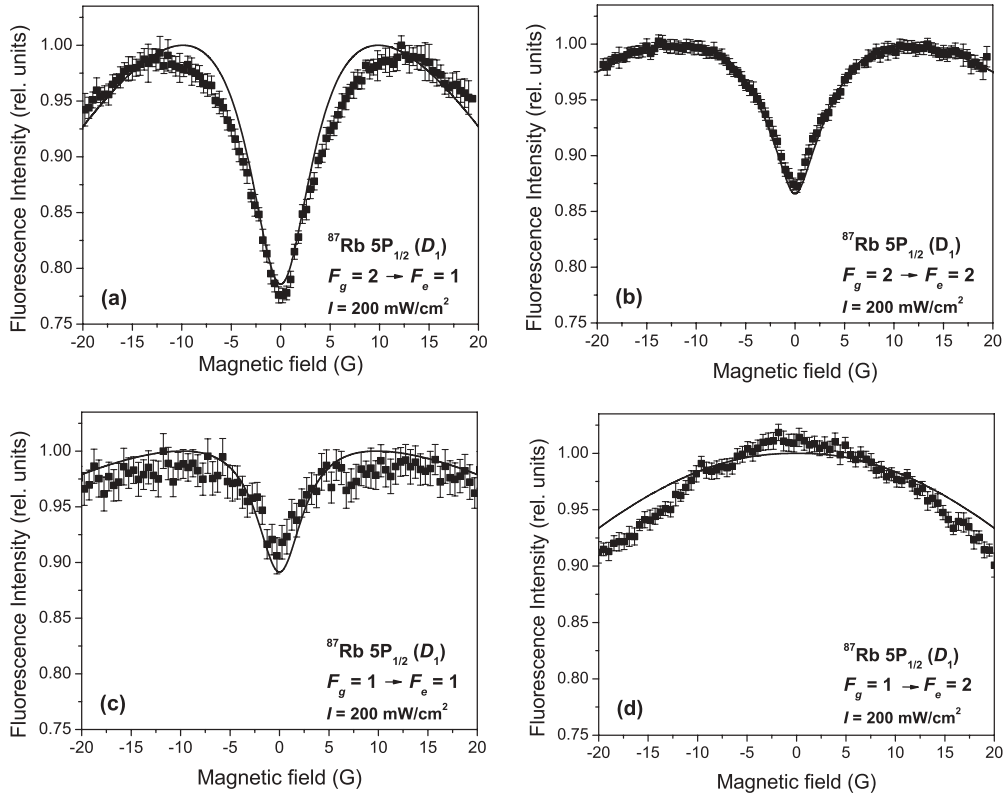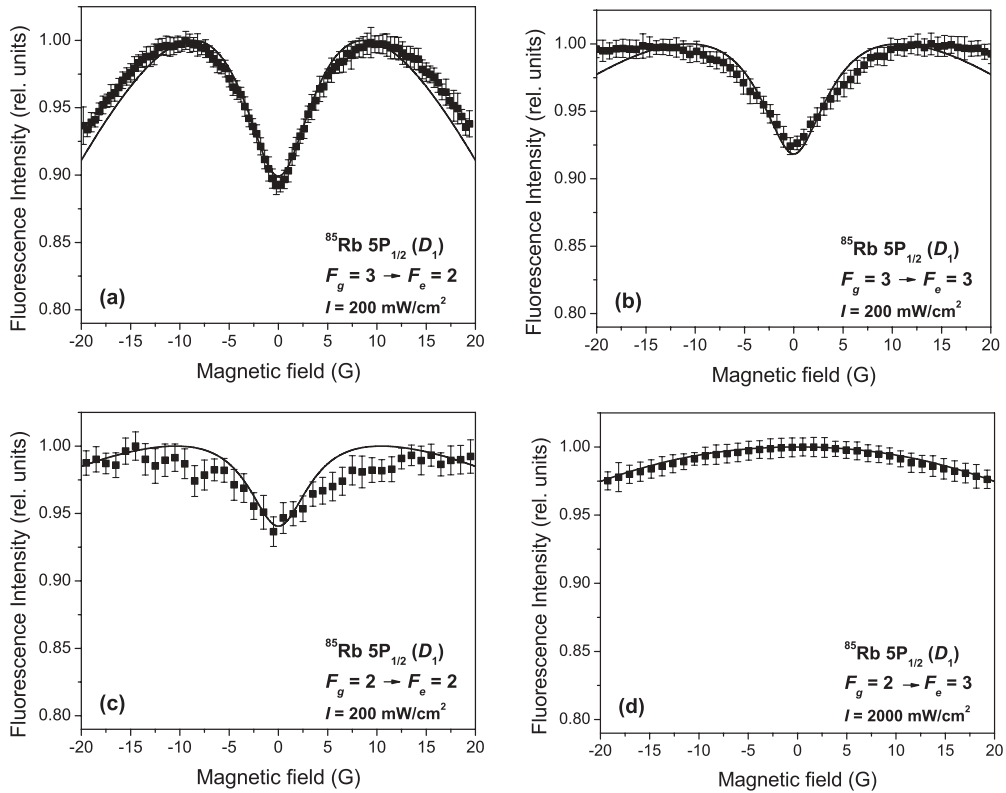
FIG. 5. Fluorescence intensity versus magnetic field for ^{87}Rb at D_1 excitation. (Filled squares) Experiment; (solid line) theory. The excited state and total angular momentum of the ground F_g and excited states F_e of the transition and laser power density I are given in each panel. ETC wall separation L is equal to λ, the wavelength of the light.

FIG. 6. Fluorescence intensity versus magnetic field for ^{85}Rb at D_1 excitation. (Filled squares) Experiment; (solid line) theory. The excited state and total angular momentum of the ground F_g and excited states F_e of the transition, and laser power density I are given in each panel. $L = \lambda$.
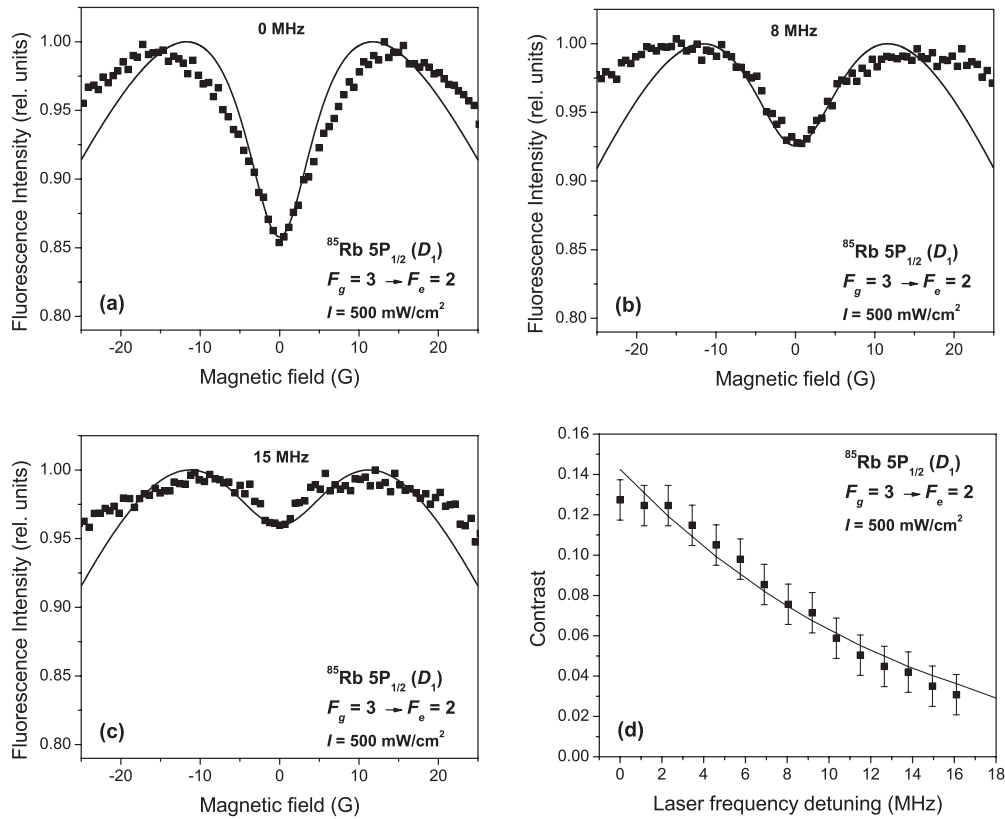
FIG. 7. (a)–(c) Fluorescence intensity versus magnetic field for the $F_g = 3 \rightarrow F_e = 2$ transition of ^{85}Rb at D_1 excitation at various values of the laser detuning with respect to the exact position of the $F_g = 3 \rightarrow F_e = 2$ transition; (d) resonance contrast versus laser frequency detuning. (Filled squares) Experiment; (solid line) theory. $L = \lambda$.

is sensitive to detuning [9]. The ETC should be much more sensitive to detuning because of its sub-Doppler characteristics. Figure 7 depicts the $F_g = 3 \rightarrow F_e = 2$ transition of ^{85}Rb for various values of the detuning from the point of maximum fluorescence between 0 and 16 MHz. The theoretical model takes into account that the ground-state relaxation rate γ_g increases linearly with the detuning Δ as different velocity groups in the Doppler profile are selected following the relation $\gamma_g = \gamma_0 + 0.3\Delta$, with $\gamma_0 = 2.88$ MHz. As in the case of the ordinary cell, the contrast decreased as the laser was detuned from the resonance, but in the ETC the effect was much more dramatic. In the ETC, a detuning of only 20 MHz resulted in a reduction in the contrast of the dark resonance that was comparable to the reduction observed in the ordinary cell for a detuning of 300 MHz [9] at the $F_g = 3 \rightarrow F_e = 2$ transition of ^{85}Rb. The theoretically calculated curve does not describe the large-field behavior particularly well, but it does describe very well the change in contrast as a function of detuning, as can be seen especially in Fig. 7(d).

Among the parameters that one must know in order to fit the resonance shapes is the Rabi frequency Ω_R, which is related to the laser power density I as $I = k_{\text{Rabi}}\Omega_R^2$. Figure 8 shows the $F_g = 2 \rightarrow F_e = 1$ transition of ^{87}Rb at various laser power densities. The filled squares show the results of the experiment, whereas the solid line shows the result of the theoretical calculation. Figure 9 shows the measured and calculated resonance contrasts for all dark resonances of the rubidium D_1 transition. Similar to the case of the ordinary cell,

the resonance contrast and width increased with increasing Rabi frequency, but the increase reaches a maximum at higher Rabi frequencies and then diminishes.

The model assumed a residual Doppler width in the direction transverse to the ETC walls on order of 60 MHz (FWHM) for all calculations corresponding to wall separation $L = \lambda$. This Doppler width corresponds to the value obtained by fitting a Voigt profile to the LIF excitation spectrum for $L = \lambda$ (similar to Fig. 2, except that in Fig. 2, $L = \lambda/2$.) The Doppler width in the direction transverse to the ETC walls was therefore about 10 times less than the Doppler width in the directions parallel to the walls at the ETC temperature. Such a Doppler width is consistent with the value of the ground-state relaxation rate γ_g assumed to achieve the best fit with the experimental data, if one assumes that the ground-state relaxation rate is related to the typical time of flight before an atom collides with one of the ETC walls.

Since the ETC cell walls are inclined toward each other, it is possible to perform the experiment at different wall separations. The approximate wall separation L can be inferred from the constructive [$L = (2n + 1)\lambda/4$] or destructive ($L = n\lambda/2$) interference of the laser beams of wavelength λ reflected from the ETC's two inside walls. Figure 10 shows the laser-induced fluorescence intensity versus the magnetic field for $L = \lambda/2$, $L = 3\lambda/4$, $L = \lambda$, and $L = 3\lambda/2$. The theoretical curves are calculated with the residual Doppler width, the ground-state relaxation time γ_g^{-1}, and the excited-state relaxation time γ_e^{-1} all linearly proportional to the wall separation, which
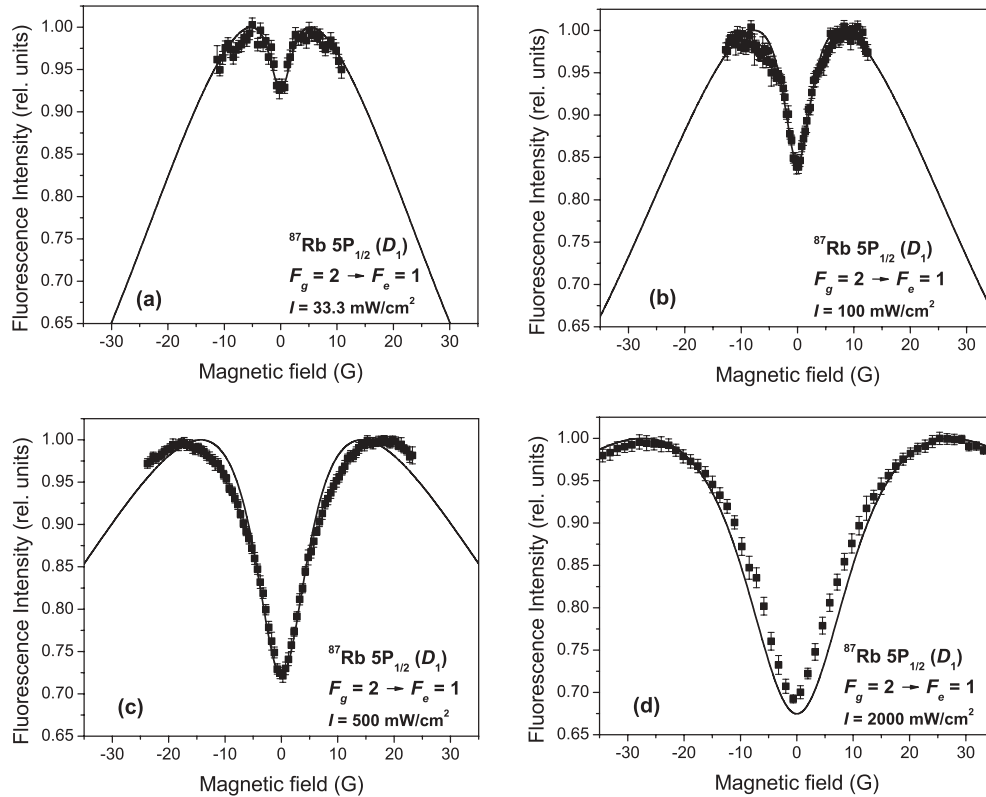
FIG. 8. Resonance signals for ^{87}Rb at the $F_g = 2 \rightarrow F_e = 1$ transition for different laser power densities I. (Filled squares) Experiment; (solid line) theory. $L = \lambda$.

seems reasonable in the case of the ETC. The LIF-induced background was assumed to be 67% for $L = \lambda/2$, 57% for $L = 3\lambda/4$, and 50% for $L = \lambda$ and $L = 3\lambda/2$. The calculated curves follow the trend of the experimentally measured curves. However, in order to obtain a satisfactory fit, it was necessary to assume that the Rabi frequency is modified by the small wall separation. Thus, an effective Rabi frequency was also adjusted until the best fit could be obtained. Interestingly, Fig. 10 suggests that the effective Rabi frequency used in the fit is linearly proportional to the cell thickness, and the fit of the Rabi frequencies versus wall thickness passes very close to the origin. Other parameters included were 10 MHz

for the laser linewidth as well as the atomic parameters from Refs. [17,18].

In general the theoretical calculations did a reasonably good job in reproducing the resonance contrasts over a wide range of different experimental conditions and for four distinct hyperfine transitions in each of two isotopes. However, the agreement achieved between theory and experiment in the ETC was somewhat less satisfactory than in the case of the ordinary cell [9], because in the ETC it was not possible to use the same background and conversion between Rabi frequency and laser power density for all transitions. At high Rabi frequencies, the model also ceases to work as well, just as was the case for
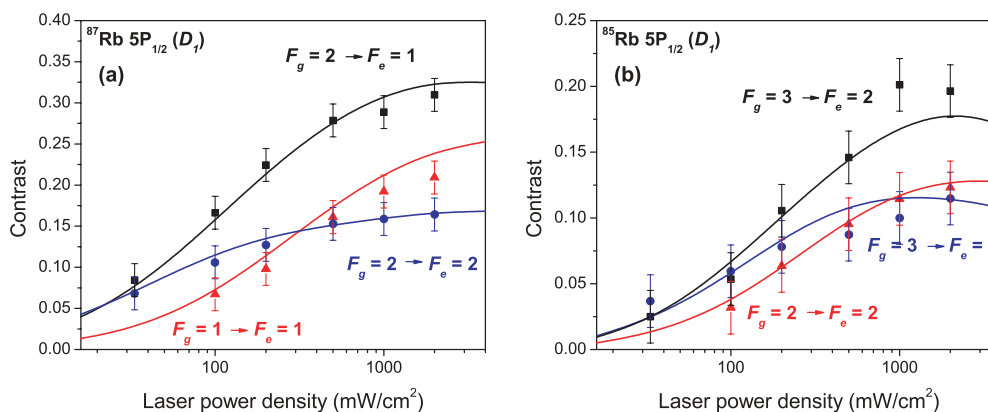

FIG. 9. (Color online) Resonance contrast as a function of laser power density for (a) ^{87}Rb and (b) ^{85}Rb dark resonances. (Markers) Experiment; (solid line) theory. $L = \lambda$.
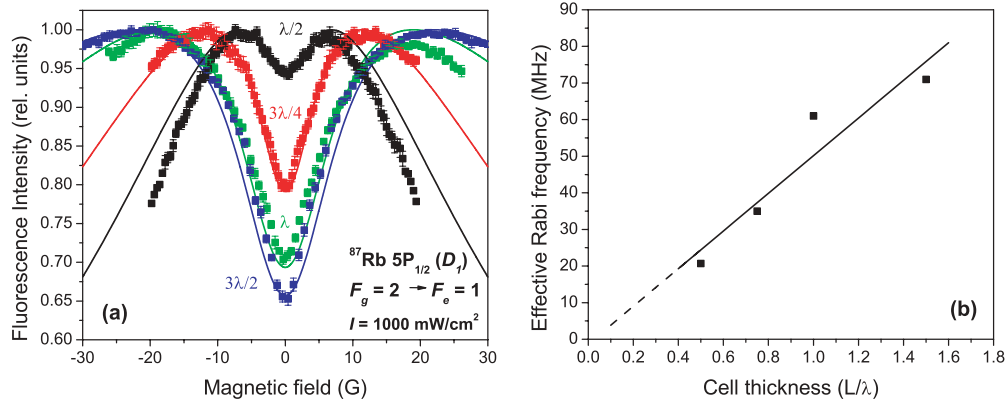
FIG. 10. (Color online) (a) Fluorescence intensity versus magnetic field at various values of the wall separation for the $F_g = 2 \rightarrow F_e = 1$ transition of ^{87}Rb. (Markers) Experiment; (solid line) theory. (b) Effective Rabi frequency used in model to calculate (a) versus cell thickness.

the ordinary cells (see Fig. 9 in Ref. [9]). Furthermore, the agreement at large fields is also not perfect for all transitions. The inclusion in the model of mixing of magnetic sublevels in the magnetic field turns out to be a small effect that cannot significantly improve the large field results. For example, even at a magnetic field of 60 G, magnetic field mixing of the excited state of ^{85}Rb changes the signals by only 0.5%.

There are several factors that could explain discrepancies between theory and experiment in the ETC. For one thing, the resonances in the ETC are very sensitive to laser detuning (see Fig. 7). Thus, the inevitable small drift of the laser frequency during a single measurement or between measurements, which had negligible impact on the results in the ordinary cell, had a greater impact on the results of the ETC. Also, the ETC cell thickness is a rapidly changing and nonlinear function of position. The neutral density filters used to obtain different laser power densities could displace the laser beam slightly to an area with a different cell thickness and hence relaxation times. Furthermore, the laser beam was about 0.4 mm in diameter, and so the ETC thickness was not constant within the laser beam. On the other hand, the model was able to describe the data in the ETC at higher laser power densities, because in the ETC, which has a larger ground-state relaxation rate, the saturation parameter $\Omega_R^2/(\Gamma \gamma_g)$ is smaller than in the ordinary cell for the same Ω_R^2.

It should be noted that the experimental dependence on the frequency detuning Δ of the width and contrast of the dark resonances formed in the ETC (Fig. 7) were in agreement with the results of the dark resonance formation in an ETC in a Λ system with two lasers (^{85}Rb $5S_{1/2}, F_g = 2 \rightarrow 5P_{3/2} \rightarrow 5S_{1/2}, F_g = 3$) [28,29]. Namely, as the coupling laser was detuned from the resonance with an atomic transition, a strong increase of the resonance width of the electromagnetically induced transparency and a worsening of the contrast were recorded. In ordinary cm-size cells, effectively the opposite behavior would be observable.

When the coupling laser frequency was in exact resonance with corresponding atomic transition in the above mentioned case of the formation of dark resonances in a Λ system in an ETC, a weak dependence of the dark resonance width on L (as $\sim 1/L^{1/4}$) was observed [1]. The dependence of linewidth

on L presented in Fig. 10 was somewhat stronger. This could have been caused by a rapid increase of the width of the dark resonance ($\sim 1/L$) as the thickness decreased for the case of large Δ [1].

V. CONCLUSION

Nonlinear magneto-optical resonances have been measured for all hyperfine transitions of the D_1 line of ^{85}Rb and ^{87}Rb in an ETC under a wide variety of experimental conditions, which included different laser power densities, laser detunings, and ETC thicknesses. Dark resonances have been observed as expected for all hyperfine transitions with $F_g \geqslant F_e$. Bright resonances were not observed for the transitions with $F_g < F_e$, which was consistent with the theoretical predictions. One of the main differences between these resonances in the ETC and the resonances in an ordinary vapor cell was that resonances in an ETC were substantially broader and had smaller contrast. The experimental signals were described with a theoretical model that was based on the optical Bloch equations and which had been used previously to describe successfully these types of resonances in ordinary vapor cells. Compared to more complex models (see, for example, Ref. [7]), our model achieved better agreement when values for the model parameters were used that corresponded to the particular characteristics of the ETC. The theoretical model suggested that the ground-state relaxation rate γ_g was a key parameter for describing the signals, but that its value in the ETC depended on the ETC wall separation instead of on the laser beam diameter, as in ordinary vapor cells. Furthermore, in order to obtain the best possible agreement between theory and experiment, it was necessary to introduce an additional excited-state relaxation rate γ_e that was related to the ETC wall separation, and which was negligible in the model for the ordinary cell. It was also necessary to introduce an effective Rabi frequency that depended on wall separation. The best-fit parameters indicated that the atoms in the ETC had a residual Doppler distribution in the direction perpendicular to the cell walls that was on the order of 60 MHz (FWHM), which was consistent with a ground-state relaxation rate based on wall collisions.

The results showed that it is possible to describe some aspects of nonlinear magneto-optical resonances in ordinary cells and ETCs over a wide range of experimental conditions with the same theoretical model, which was based on the optical Bloch equations, averaged over the Doppler profile, included all neighboring hyperfine transitions, took into account the splitting and mixing of the magnetic sublevels in an external magnetic field, and treated the coherence properties of the radiation field. As a result, this theoretical model can serve as a tool for future investigations with ETCs and for the development of practical applications based on them. It should be noted that the conditions of the ETC may not be stationary as in the case of ordinary cells. Our attempt to account for nonstationary behavior by introducing an effective Rabi frequency that depends on the wall separation probably could be improved in the future by a more detailed model. The remaining discrepancies between theory and experiment suggest that there do exist additional physical effects that should be taken into account or treated in greater detail in the theoretical description of the ETC.

[1] D. Sarkisyan and A. Papoyan, *Optical Processes in Micro- and Nanometric Thin Cells Containing Atomic Vapor*, Horizons in World Physics, Vol. 263 (Nova Science Publishers, Hauppage, NY, 2009), chap. 3, pp. 85.

[2] A. Sargsyan, G. Hakhumyan, A. Papoyan, D. Sarkisyan, A. Atvars, and M. Auzinsh, Appl. Phys. Lett. **93**, 021119 (2008).

[3] D. Sarkisyan, D. Bloch, A. Papoyan, and M. Ducloy, Opt. Commun. **200**, 201 (2001).

[4] G. Alzetta, A. Gozzini, L. Moi, and G. Orriols Il, Nuovo Cimento B **36**, 5 (1976).

[5] R. W. Schmieder, A. Lurio, W. Happer, and A. Khadjavi, Phys. Rev. A **2**, 1216 (1970).

[6] Y. Dancheva, G. Alzetta, S. Cartalava, M. Taslakov, and C. Andreeva, Opt. Commun. **178**, 103 (2000).

[7] C. Andreeva, A. Atvars, M. Auzinsh, K. Blush, S. Cartaleva, L. Petrov, and D. Slavov, Phys. Rev. A **76**, 063804 (2007).

[8] M. Auzinsh, R. Ferber, F. Gahbauer, A. Jarmola, and L. Kalvans, Phys. Rev. A **78**, 013417 (2008).

[9] M. Auzinsh, R. Ferber, F. Gahbauer, A. Jarmola, and L. Kalvans, Phys. Rev. A **79**, 053404 (2009).

[10] D. Budker, W. Gawlik, D. F. Kimball, S. M. Rochester, V. V. Yashchuk, and A. Weis, Rev. Mod. Phys. **74**, 1153 (2002).

[11] J.-C. Lehmann and C. Cohen-Tannoudji, C. R. Acad. Sci. Paris Ser. IV **258**, 4463 (1964).

[12] M. Ducloy, M. P. Gorza, and B. Decomps, Opt. Commun. **8**, 21 (1973).

[13] W. Gawlik, J. Kowalski, R. Neumann, and F. Träger, Opt. Commun. **12**, 400 (1974).

[14] J. L. Picqué, J. Phys. B: Atom. Molec. Phys. **11**, L59 (1978).

[15] K. Blushs and M. Auzinsh, Phys. Rev. A **69**, 063806 (2004).

[16] A. V. Papoyan, M. Auzinsh, and K. Bergmann, Eur. Phys. J. D **21**, 63 (2002).

[17] D. A. Steck, *Rubidium 85 d line data* (2009), revision 2.1.2, 12 August 2009, http://steck.us/alkalidata.

[18] D. A. Steck, *Rubidium 87 d line data* (2009), revision 2.1.2, 12 August 2009, http://steck.us/alkalidata.

[19] C. Andreeva, S. Cartaleva, Y. Dancheva, V. Biancalana, A. Burchianti, C. Marinelli, E. Mariotti, L. Moi, and K. Nasyrov, Phys. Rev. A **66**, 012502 (2002).

[20] S. Stenholm, *Foundations of Laser Spectroscopy* (Dover, Mineoloa, NY, 2005).

[21] L. Allen and J. H. Eberly, *Optical Resonance and Two Level Atoms* (Wiley, New York, 1975).

[22] N. G. van Kampen, Phys. Rep. **24**, 171 (1976).

[23] G. Breit and I. I. Rabi, Phys. Rev. **38**, 2082 (1931).

[24] E. B. Aleksandrov, M. Chaika, and G. I. Khvostenko, *Interference of Atomic States* (Springer Verlag, Berlin, 1993).

[25] A. P. Kazantsev, V. S. Smirnov, A. M. Tumaikin, and I. A. Yagofarov, Opt. Spectrosc. (USSR) **57**, 116 (1984) [Opt. Spektrosk. **57**, 189 (1984)].

[26] F. Renzoni, S. Cartaleva, G. Alzetta, and E. Arimondo, Phys. Rev. A **63**, 065401 (2001).

[27] J. Alnis and M. Auzinsh, Phys. Rev. A **63**, 023407 (2001).

[28] A. Sargsyan, D. Sarkisyan, and A. Papoyan, Phys. Rev. A **73**, 033803 (2006).

[29] Y. Pashayan-Leroy, C. Leroy, A. Sargsyan, A. Papoyan, and D. Sarkisyan, J. Opt. Soc. Am. B **24**, 1829 (2007).